Generation of passively *Q*-switched fiber laser at 1 μm by using MoSSe as a saturable absorber

H. Ahmad*, S. A. Reduan, S. N. Aidit, and Z. C. Tiu

Photonics Research Centre, University of Malaya, Kuala Lumpur 50603, Malaysia
**Corresponding author: harith@um.edu.my*

Received October 5, 2016; accepted November 23, 2016; posted online December 27, 2016

Passively *Q*-switched ytterbium-doped fiber lasers (YDFLs) incorporating a molybdenum sulfide selenide (MoSSe)-based saturable absorber (SA) are demonstrated. The modulation depth and saturation intensity of the MoSSe-based SA are measured to be approximately 25.0% and 0.002 MW/cm^2, respectively, using the twin detector technique. The YDFL's output has a center wavelength of 1038.5 nm with a top pulse width and energy of 1.2 μs and 18.9 nJ, respectively, at a pump power of 333 mW. The MoSSe-based SA has a good linear optical response, providing significant opportunity for use in applications over an ultra-broadband spectrum, particularly spectroscopy and biomedical diagnostics.

OCIS codes: 060.0060, 060.2310, 060.3510, 060.4370.
doi: 10.3788/COL201715.020601.

Fiber lasers capable of passively generating *Q*-switched pulses are the focal point of substantial research efforts due to their wide range of applications, including range finding, material processing, and optical communication[1]. *Q*-switching in fiber lasers can be achieved passively through the use of saturable absorbers (SAs), including semiconductor SA mirrors[2,3] and transition-metal-doped crystals[4], as well as graphene, carbon nanotubes (CNTs), and their derivatives[5–7]. Graphene was initially seen as a highly promising material to be used as an SA for generating *Q*-switched pulses but exhibits a weak absorption capability of around 2.3% per layer, which in turn limits the modulation co-efficiency of graphene-based SAs[8]. Similar to graphene, CNTs, which are another carbon derivative, also have the potential to be good candidates as SAs, but the combination of different CNT diameters necessary for broadband operation leads to the high non-saturable losses as a result of the non-resonance effect by large numbers of CNTs[8].

As a result of this, research has now focused on the exploration of new materials for use as SAs. Among the materials being explored are topological insulators (TIs), such as (Bi_2Se_3)[9–13] and bismuth telluride (Bi_2Te_3)[14,15], which have already seen applications in various *Q*-switched fiber laser designs. Another potential material is transition metal dichalcogenides (TMDs). TMDs encompass various transition metal compounds, such as molybdenum sulfide (MoS_2)[16–18], molybdenum diselenide ($MoSe_2$)[19], tungsten disulfide (WS_2)[20–22], and tungsten diselenide (WSe_2)[23], and have been successfully demonstrated in *Q*-switched fiber laser operations. TMDs in particular exhibit layer-dependent optical properties and, at near-infrared wavelengths, have the ability to alternate their bandgap between indirect and direct, making them highly desirable as optical materials[24]. Furthermore, TMDs have high non-linearity, ultrafast carrier dynamics, great photoluminescence, and strong absorption, making them suitable for a variety of photonic applications[25,26].

Of the many TMDs, however, one TMD, molybdenum sulfide selenide (MoSSe), has received little attention in the study of SAs. As MoSSe hails from the same family as other TMDs, it is predicted that it would exhibit the same characteristics as other TMD-based SAs and thus have potential to be applied to passively generating *Q*-switched pulses in fiber lasers. It is interesting to note that MoSSe is the amongst the most stable TMDs as a result of its ordered alloy structures. The reported MoSSe bandgap is only 0.05 eV due to size and chemical differences between two constituent elements[27], although this suggests that the TMD monolayer bandgap could be varied by altering the X_2 composition, unlike MoS_2 or $MoSe_2$[28].

In this work, a *Q*-switched fiber laser using an MoSSe-based SA operating in the 1.0 to 1.5 μm region is presented. The MoSSe's non-linear absorption characteristics are obtained by the twin detector technique, and the results indicate modulation depths of ~25% and ~0.002 MW/cm^2 at 1560 nm. The fiber laser can generate output pulses with a narrow pulse width of 1.2 μs and a corresponding pulse energy of 18.9 nJ. To the best of authors knowledge, this is the first report of an MoSSe-based SA being used to achieve a *Q*-switching operation at the 1.0 region and indicates the potential for MoSSe to be used as a broadband SA for generating passively *Q*-switched pulses in a fiber laser system.

The MoSSe-based SA used here was prepared using the mechanical exfoliation technique. This process is illustrated in Fig. 1. In this technique, a piece of scotch tape is prepared, as is a small MoSSe crystal flake, as shown in Fig. 1(a). Next, the MoSSe crystal flake is carefully placed on the scotch tape, and scotch tape is folded in two, as shown in Figs. 1(b) and 1(c), respectively. The folded scotch tape is repeatedly pressed to exfoliate a few MoSSe

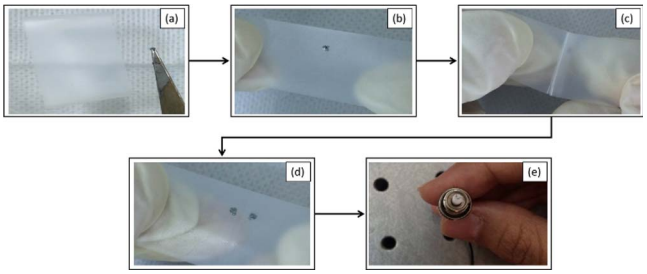

Fig. 1. MoSSe mechanical exfoliation process and deposition onto the fiber ferrule.

layers on the other side of the scotch tape. Figure 1(d) shows the thin MoSSe layer obtained on the other side of the scotch tape once it is unfolded. The thin MoSSe layers are then carefully removed and placed onto the surface of a fiber ferrule before being embedded with an index matching gel as per Fig. 1(e).

The characterization of the MoSSe Raman is in Fig. 2. The linear and non-linear optical characteristics and the microscope image of the MoSSe is shown in Figs. 2(a)–2(c), respectively. Raman spectroscopy at a wavelength of 532 nm using an $1800:l/mm$ grating reveals the Raman spectrum of the MoSSe SA. It can be seen from the spectrum obtained that two primary peaks are seen at 210 and 260 cm^{-1}, indicating the presence of Mo-Se. Additionally, a single secondary peak at approximately 400 cm^{-1} is also observed, indicating the presence of the compound Mo-S. These findings are comparable to those reported by Konkena *et al.*[29], and augur well with their report in which the inclusion of the Se element weakens the Mo-S band within the MoSSe structure, thus giving different peaks as compared to those acquired for MoS_2 and $MoSe_2$. Furthermore, the shift in the Raman peak indicates the sample layer to be about 5 to 6 layers, or about 6 nm thick.

For the characterization of the MoSSe's linear optical characteristics, a white light source with a wavelength range from 900 to 1600 nm is used. Figure 2(a) shows

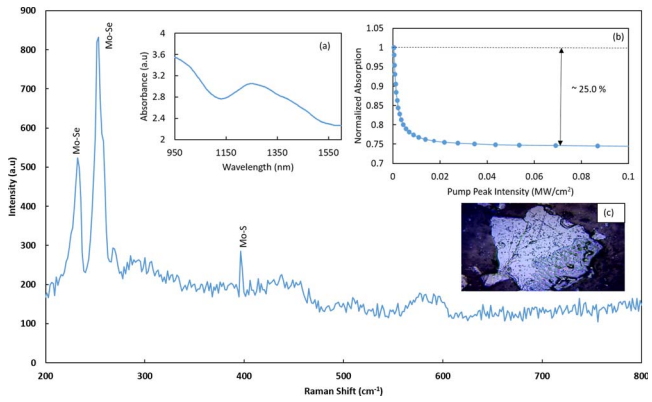

Fig. 2. Characterization of MoSSe SA Raman spectrum. The insets of Fig. 2 show (a) the linear absorption, (b) the non-linear absorption measurement, and (c) the microscope image capture of the SA.

the linear optical response of the MoSSe sample, covering a range of 1150 to about 1450 nm. It is interesting to observe that when it is exposed to light at 900 nm, the linear response of the MoSSe sample is significant, with an absorbance of almost 3.6 a.u. However, the absorbance decreases as the wavelength of the light source increases, reaching a dip of about 2.8 a.u. at about 1150 nm before rising again and peaking at an absorbance value of 3.0 a.u. at a wavelength 1250 nm, before finally dropping again. This indicates that the optimum operating region for the MoSSe is between 1000 and 1500 nm, making it suitable for operation in the C-band and particularly the S-band regions.

The inset of Fig. 2(b), on the other hand, shows the MoSSe-based SA's nonlinear optical absorption. For this measurement, the twin detector technique is used, and the collected data are fitted into the saturation model formula[30–32]. A mode-locked seed laser with a 1560 nm center wavelength is used for the twin detector technique, and the measured modulation depth and saturation intensity are approximately 25.0% and 0.002 MW/cm^2, respectively. The modulation depth obtained is comparable to those previously reported by Li *et al.*[33], Chen *et al.*[34], Du *et al.*[35], and Lu[36] on two-dimensional (2D) nanomaterials. Figure 2(c) shows the actual MoSSe-based SA, with the MoSSe sample sitting on the fiber ferrule as captured using a microscope.

The proposed fiber laser's schematic is given in Fig. 3. The proposed system uses a length of 0.7 meter (Fibercore DF1100) ytterbium-doped fiber (YDF) as the active gain medium, which is excited by a laser diode (LD) operating at 974 nm with a maximum pump power of 333 mW. The YDF has an operating wavelength of between 1030 and 1100 nm with cutoff wavelengths of 800–900 nm, as well as a numerical aperture (NA) between 0.14 and 0.17 and a nominal absorption of 1500 dB/m at 975 nm. The LD is connected to the YDF through the 980 nm port of a 980/1000 wavelength division multiplexer (WDM), with the WDM's common port connected to one end of the YDF. The YDF's other end is connected to an optical isolator, which ensures unidirectional propagation as well as blocking back-reflections within the cavity, which could be detrimental to the LD. Immediately after the optical isolator, the MoSSe-based SA is incorporated into the

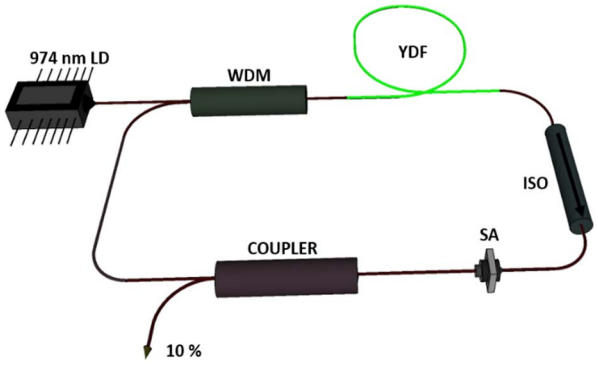

Fig. 3. Setup of the proposed Q-switched YDF laser.

laser cavity's configuration. The output from the SA is then linked to a 90∶10 optical coupler (OC), which is used to obtain a portion of the signal propagating within the cavity for analysis purposes. The 90% port of the OC is now connected to the WDM's 1000 nm port, thus completing the optical cavity.

The extracted signal is further split into two portions of equal power by a 3 dB coupler, allowing both the optical and electronic characteristics of the output pulses to be analyzed simultaneously. The cavity's total length is 13.0 m.

Measurement of the output pulses' optical characteristics is done by an optical spectrum analyzer (OSA) and indicates the occurrence of spectral broadening due to self-phased modulation. The central wavelength of the pulses is at approximately 1038.5 nm. Figure 4(a) provides the optical spectrum obtained at a pump power of 333 mW, with a measured full width at half-maximum of 2.1 nm. The inset of Fig. 4(a) shows the train of the output pulses obtained at the same pump power, taken from a radio frequency spectrum analyzer (RFSA) at a resolution of 100 Hz. A single pulse is also captured, as shown in Fig. 4(b), which gives a signal-to-noise ratio of around 45 dB for the generated peaks. This shows that the output pulses are highly stable[37] and comparable to those obtained using other types of SAs in similar configurations[1,38,39]. Furthermore, expanding the frequency span until 1 MHz, as shown as the inset of Fig. 4(b), shows the harmonics obtained by the pulses up to the thirteenth harmonic.

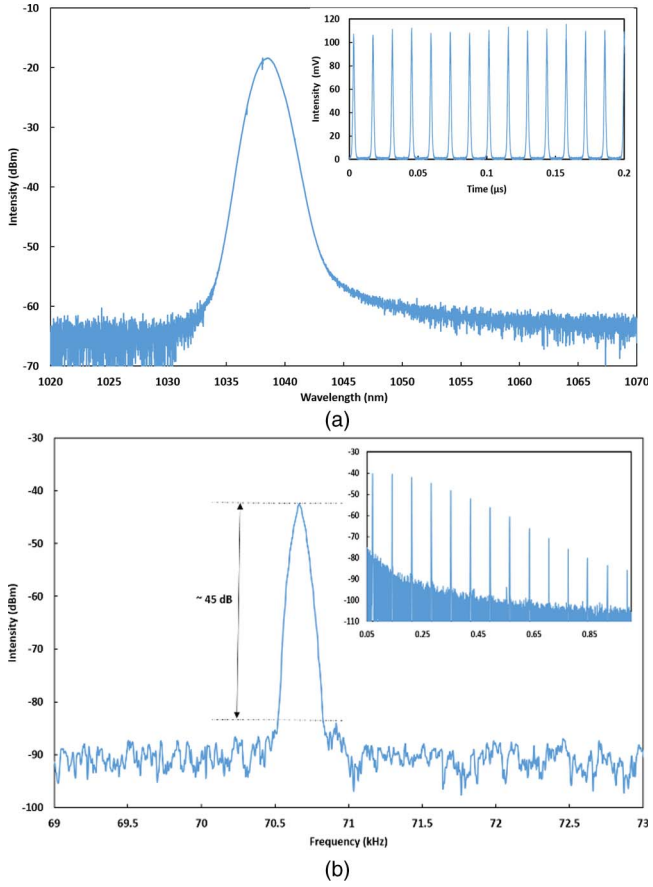

Fig. 4. Q-switched pulsed output at 1 μm, showing (a) the optical output as obtained using an OSA and a Q-switched pulse train obtained using an RFSA (inset) and (b) single-pulse RFSA and wide-band RFSA (inset).

Figure 5(a) shows the repetition rate and pulse duration of the output pulses of the proposed laser. It can be seen from the figure that the repetition rate and pulse duration increase and decrease, respectively, against the increasing pump power[40]. As the pump power is increased from 181 to 333 mW, the repetition rate responds linearly from 56.7 to 71.3 kHz, while the pulse duration is reduced at an almost linear rate as well from 2.14 to 1.2 μs. In the same manner, raising the pump power also results in the output power and pulse energy also increasing linearly, with the output power rising from 0.6 to 1.3 mW for the same rise in the pump power, as shown in Fig. 5(b). Furthermore, the pulse energy also increases linearly, as it is a function of the output power divided by the repetition rate[41], both of which increase linearly as well against the pump power. The maximum pulse energy of the system is 18.9 nJ.

From the aforementioned results, the MoSSe-based SA is highly suited for the generation of Q-switched pulses at the 1000 nm region, with the fiber laser in this work operating at a wavelength of 1038.5 nm. It is also important to note that even at the maximum pump power, the SA does

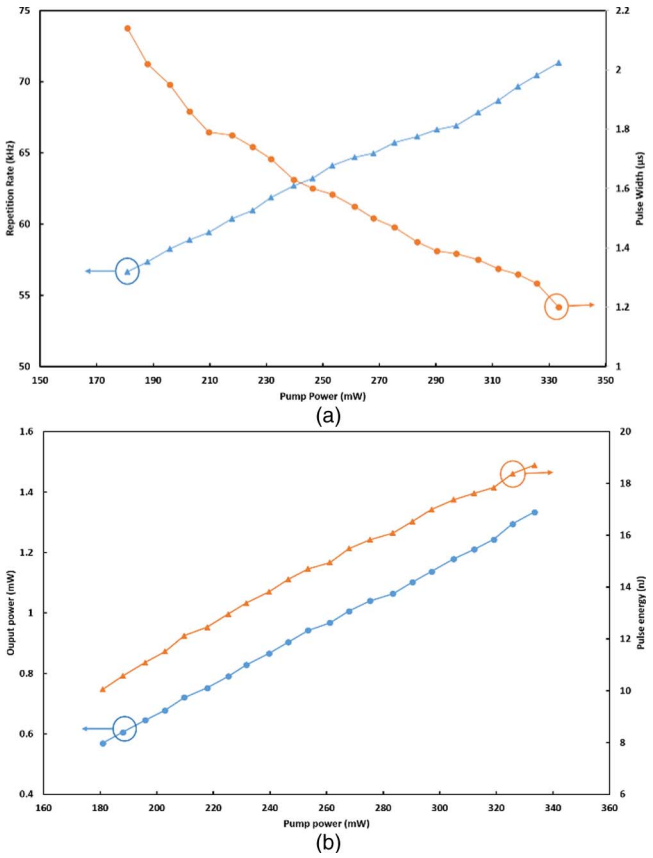

Fig. 5. (a) Repetition rate and pulse width and (b) output power and pulse energy as a function of the rising pump power.

Table 1. Comparison of Reported Work with Results of Similar Systems from Other Works Using Different SAs

Type of SA	Repetition Rate (kHz)	Min. Pulse Width (μs)	Max. Pulse Energy (nJ)	Max. Output Power (mW)	Refs.
Graphene	140–257	0.07	46	12	[43]
TI	8.3–29.1	1.95	17.9	0.46	[42]
MoS_2	6.4–28.9	5.8	32.6	0.9	[1]
MoSSe	56.7–71.3	1.2	18.9	1.3	Reported

not exhibit any signs of optical damage, as the generated pulses are highly stable and show a limited, if any, fluctuations. Furthermore, reducing and increasing the pump power result in similar results being obtained, further validating that the SA has not been damaged. Due to the lack of higher-power pump sources in this work, the damage threshold of the MoSSe-based SA could not be determined but is ascertained to be higher than 333 mW. This SA was then repeated after a few days and found to maintain its performance characteristics.

Table 1 shows the comparison between the reported results of this work with previously published results of similar systems using different SAs with the gain medium of a YDF. It can be seen that barring the graphene-based SA[41], the proposed MoSSe-based SA performs comparably against other SA types, including those fabricated from TIs[42] and other TMDs[1,33].

This work proves the capability of the MoSSe-based SA to generate Q-switched outputs in the 1000 nm region and also opens the possibility for a similar laser operating in the mode-locked regime by modifying sufficient parameters, such as the losses in the cavity and the SA's modulation depth. However, it should be noted that in this work, the thickness of the SA layer, which is approximately 5 to 6 layers thick, may not support mode locking. The proposed SA shows substantial potential for an ultrabroadband operation, as initial testing of its optical response shows similar behaviors at longer wavelengths, making it a possible candidate for various applications, including spectroscopy and biomedical diagnostics. Further applications can also be realized by incorporating a tunable bandpass filter into the setup, allowing the Q-switched output wavelength to be tuned.

In this work, a passively Q-switched YDFL using a MoSSe-based SA operating at the 1000 nm wavelength region is proposed and demonstrated. Measurement of the MoSSe based SA's nonlinear absorption by the twin detector technique provides a modulation depth of ~25.0% and saturation intensity of ~0.002 MW/cm^2. At a central wavelength of 1038.5 nm and a maximum pump power of 333 mW, a minimum pulse width and a maximum pulse energy of 1.2 μs and 18.9 nJ, with a corresponding repetition rate from 56.6 to 71.3 kHz, are obtained. The proposed MoSSe-based SA shows significant promise for various SA applications along an ultra-broadband spectrum, owning to its somewhat similar optical response characteristics at longer wavelengths, and can be a potential candidate for a multitude of applications, including spectroscopy and biomedical diagnostics.

We would like to acknowledge the University of Malaya for funding this work under the Grants LRGS (2015) NGOD/UM/KPT, GA010-2014 (ULUNG), and RU010-2016.

References

1. Z. Luo, Y. Huang, M. Zhong, Y. Li, J. Wu, B. Xu, H. Xu, Z. Cai, J. Peng, and J. Weng, J. Lightwave Technol. **32**, 4679 (2014).
2. G. Spühler, R. Paschotta, M. Kullberg, M. Graf, M. Moser, E. Mix, G. Huber, C. Harder, and U. Keller, Appl. Phys. B **72**, 285 (2001).
3. X. Shi-Xiang, L. Wen-Xue, H. Qiang, Z. Hui, and Z. He-Ping, Chin. Phys. Lett. **25**, 548 (2008).
4. J. Dong, P. Deng, Y. Liu, Y. Zhang, J. Xu, W. Chen, and X. Xie, Appl. Opt. **40**, 4303 (2001).
5. H. Ahmad, F. Muhammad, M. Zulkifli, and S. Harun, IEEE Photon. J. **4**, 2205 (2012).
6. H. Ahmad, M. Soltanian, M. Alimadad, and S. Harun, Laser Phys. **24**, 105101 (2014).
7. H. Zhang, D. Tang, L. Zhao, Q. Bao, and K. Loh, Opt. Express **17**, 17630 (2009).
8. A. Martinez and Z. Sun, Nat. Photon. **7**, 842 (2013).
9. C. Zhao, H. Zhang, X. Qi, Y. Chen, Z. Wang, S. Wen, and D. Tang, Appl. Phys. Lett. **101**, 211106 (2012).
10. C. Zhao, Y. Zou, Y. Chen, Z. Wang, S. Lu, H. Zhang, S. Wen, and D. Tang, Opt. Express **20**, 27888 (2012).
11. T. Pinghua, Z. Xiaoqi, Z. Chujun, W. Yong, Z. Han, S. Deyuan, W. Shuangchun, T. Dingyuan, and F. Dianyuan, IEEE Photon. J. **5**, 1500707 (2013).
12. H. Ahmad, M. Salim, S. R. Azzuhri, M. Soltanian, and S. Harun, Laser Phys. **25**, 065102 (2015).
13. H. Ahmad, M. Salim, M. Soltanian, S. R. Azzuhri, and S. Harun, J. Mod. Opt. **62**, 1550 (2015).
14. J. Lee, J. Koo, C. Chi, and J. H. Lee, J. Opt. **16**, 085203 (2014).
15. J. Lee, M. Jung, J. Koo, C. Chi, and J. H. Lee, IEEE J. Sel. Top. Quantum Electron. **21**, 264 (2015).
16. S. Wang, H. Yu, H. Zhang, A. Wang, M. Zhao, Y. Chen, L. Mei, and J. Wang, Adv. Mater. **26**, 3538 (2014).
17. R. I. Woodward, E. J. Kelleher, R. C. Howe, G. Hu, F. Torrisi, T. Hasan, S. V. Popov, and J. R. Taylor, Opt. Express **22**, 31113 (2014).
18. H. Xia, H. Li, C. Lan, C. Li, J. Du, S. Zhang, and Y. Liu, Photon. Res. **3**, A92 (2015).
19. R. Woodward, R. Howe, T. Runcorn, G. Hu, F. Torrisi, E. Kelleher, and T. Hasan, "Wideband saturable absorption in few-layer molybdenum diselenide ($MoSe_2$) for Q-switching Yb-, Er-and Tm-doped fiber lasers," arXiv preprint arXiv:1503.08003 (2015).
20. S. H. Kassani, R. Khazaeizhad, H. Jeong, T. Nazari, D.-I. Yeom, and K. Oh, Opt. Mater. Express **5**, 373 (2015).

21. M. Zhang, G. Hu, R. Howe, L. Chen, Z. Zheng, and T. Hasan, "Yb-and Er-doped fiber laser *Q*-switched with an optically uniform, broadband WS_2 saturable absorber," arXiv preprint arXiv:1507.03188 (2015).
22. J. Lin, Y. Hu, C. Chen, C. Gu, and L. Xu, Opt. Express **23**, 29059 (2015).
23. B. Chen, X. Zhang, K. Wu, H. Wang, J. Wang, and J. Chen, Opt. Express **23**, 26723 (2015).
24. S. Wang, H. Yu, H. Zhang, A. Wang, M. Zhao, Y. Chen, L. Mei, and J. Wang, Adv. Mater. **26**, 3538 (2014).
25. J. Wilson and A. Yoffe, Adv. Phys. **18**, 193 (1969).
26. X. Huang, Z. Zeng, and H. Zhang, Chem. Soc. Rev. **42**, 1934 (2013).
27. J. Kang, S. Tongay, J. Li, and J. Wu, J. Appl. Phys. **113**, 143703 (2013).
28. S.-H. Su, W.-T. Hsu, C.-L. Hsu, C.-H. Chen, M.-H. Chiu, Y.-C. Lin, W.-H. Chang, K. Suenaga, H. He, Jr., and L.-J. Li, Front. Energy Res. **2**, 27 (2014).
29. B. Konkena, J. Masa, W. Xia, M. Muhler, and W. Schuhmann, Nano Energy **29**, 46 (2016).
30. H. Ahmad, N. Ruslan, M. Ismail, Z. Ali, S. Reduan, C. Lee, and S. Harun, Laser Phys. **26**, 095103 (2016).
31. R. I. Woodward, E. J. R. Kelleher, R. C. T. Howe, G. Hu, F. Torrisi, T. Hasan, S. V. Popov, and J. R. Taylor, Opt. Express **22**, 31113 (2014).
32. H. Zhang, S. Lu, J. Zheng, J. Du, S. Wen, D. Tang, and K. Loh, Opt. Express **22**, 7249 (2014).
33. H. Li, H. Xia, C. Lan, C. Li, X. Zhang, J. Li, and Y. Liu, IEEE Photon. Technol. Lett. **27**, 69 (2015).
34. C. Yu, Z. Chujun, C. Shuqing, D. Juan, T. Pinghua, J. Guobao, Z. Han, W. Shuangchun, and T. Dingyuan, IEEE J. Sel. Top. Quantum Electron. **20**, 315 (2014).
35. J. Du, Q. Wang, G. Jiang, C. Xu, C. Zhao, Y. Xiang, Y. Chen, S. Wen, and H. Zhang, Sci. Rep. **4**, 6346 (2014).
36. S. Lu, L. Miao, Z. Guo, X. Qi, C. Zhao, H. Zhang, S. Wen, D. Tang, and D. Fan, Opt. Express **23**, 11183 (2015).
37. D. Von der Linde, Appl. Phys. B **39**, 201 (1986).
38. Z. Yu, Y. Song, J. Tian, Z. Dou, H. Guoyu, K. Li, H. Li, and X. Zhang, Opt. Express **22**, 11508 (2014).
39. H. Ahmad, S. Reduan, Z. A. Ali, M. Ismail, N. Ruslan, C. Lee, R. Puteh, and S. Harun, IEEE Photon. J. **8**, 1 (2016).
40. U. Keller, Prog. Opt. **46**, 1 (2004).
41. M. E. Fermann, A. Galvanauskas, and G. Sucha, *Ultrafast Lasers: Technology and Applications* (CRC Press, 2002), Vol. **80**.
42. Z. Luo, Y. Huang, J. Weng, H. Cheng, Z. Lin, B. Xu, Z. Cai, and H. Xu, Opt. Express **21**, 29516 (2013).
43. J. Liu, S. Wu, Q.-H. Yang, and P. Wang, Opt. Lett. **36**, 4008 (2011).